Journal of Theoretical Biology 581 (2024) 111739

Contents lists available at ScienceDirect

Journal of Theoretical Biology

journal homepage: www.elsevier.com/locate/yjtbi

Oscillations of algal cell quota: Considering two-stage phosphate uptake kinetics

Anglu Shen [a,1], Shufei Gao [b,1], Jie Jiang [b], Qingjing Hu [c], Hao Wang [d], Sanling Yuan [b,*]

[a] College of Marine Ecology and Environment, Shanghai Ocean University, Shanghai 201306, China
[b] College of science, University of Shanghai for Science and Technology, Shanghai 200093, China
[c] Yellow Sea Fisheries Research Institute, Chinese Academy of Fishery Sciences, Qingdao 266071, China
[d] Department of Mathematical and Statistical Sciences, University of Alberta, Edmonton, Alberta T6G 2G1, Canada

ARTICLE INFO

Keywords:
Algal bloom
Prorocentrum donghaiense
Karenia mikimotoi
Surface adsorption
Transport delay
Two-stage model

ABSTRACT

Elucidating the mechanism of effect of phosphate (PO_4^{3-}) uptake on the growth of algal cells helps understand the frequent outbreaks of algal blooms caused by eutrophication. In this study, we develop a comprehensive mathematical model that incorporates two stages of PO_4^{3-} uptake and accounts for transport time delay. The model parameter values are determined by fitting experimental data of *Prorocentrum donghaiense* and the model is validated using experimental data of *Karenia mikimotoi*. The numerical results demonstrate that the model successfully captures the general characteristics of algal growth and PO_4^{3-} uptake under PO_4^{3-} sufficient conditions. Significantly, the experimental and mathematical findings suggest that the time delay associated with the transfer of PO_4^{3-} from the surface-adsorbed PO_4^{3-} (P_s) pool to the intracellular PO_4^{3-} (P_i) pool may serve as a physiologically plausible mechanism leading to oscillations of algal cell quota. These results have important implications for resource managers, enabling them to predict and deepen their understanding of harmful algal blooms.

1. Introduction

Harmful algal blooms (HABs) caused by abnormal proliferation or high biomass accumulation or other toxic microalgae at the sea surface or in the water column have brought deleterious impacts on aquaculture, fisheries, tourism, human health, and components of aquatic ecosystems (Hallegraeff, 1993; Anderson, 1997; Anderson et al., 2012). About 300 species of phytoplankton are the bloom-forming species, while only 40 or so species have the capacity to produce potent toxins, and most of them are dinoflagellates (Hallegraeff, 1993). The coastal water in the East China Sea (ECS) and Yangtze River Estuary (YRE) is one of the famous regions with frequent HABs events since the 1980s (Yu et al., 2017). The dinoflagellate *Prorocentrum donghaiense* (formerly named *P. shikokuense*; Lu and Goebel, 2001; Lu et al., 2022; Gómez et al., 2021) is a major dinoflagellate species that forms blooms in the coastal waters of the ECS each year since 2000 during late April-May (Yu et al., 2017; Lu et al., 2022). The scale (approximately 10000 km^2) and length of time (approximately one month) of the *P. donghaiense* blooms have been amazing for some years (Yu et al., 2017). Like other HABs, the blooms of *P. donghaiense* may be great harmful to the ecosystem and fishery resources. This is often due to the accumulation of algal biomass, which produces toxic scum and foam, covering other phytoplankton and sea grass beds, and causing animal death through decay and oxygen consumption (Anderson et al., 2012). Laboratory and field studies have shown that the *P. donghaiense* blooms are extremely harmful to the survival of zooplankton and scallop (Lin et al., 2015; Shen et al., 2022). Furthermore, during the *P. donghaiense* blooms, the community structure of zooplankton changes significantly, from being copepod and jellyfish-dominated to small jellyfish-dominated (Lin et al., 2014), and it is well known that copepods are the main food source for many fish larvae (Uye et al., 1999). Therefore, elucidating the growth characteristics of *P. donghaiense* will help to better understand its possible effects on the ECS and YRE ecosystems.

Due to widespread nutrient loading such as phosphate (PO_4^{3-}), the eutrophication of aquatic ecosystems throughout the world leads to the appearance of HABs (Zhou et al., 2017b; Xiao et al., 2019). In the ECS and YRE, diatom blooms and dinoflagellate blooms often appear alternatively (diatom-dinoflagellate-diatom) from April to August, where PO_4^{3-} plays an important role in this succession. Diatom blooms (such as *Skeletonema costatum*) occur in early spring when the external

* Corresponding author.
E-mail address: sanling@usst.edu.cn (S. Yuan).
[1] Co-first author.

https://doi.org/10.1016/j.jtbi.2024.111739
Received 1 June 2023; Accepted 10 January 2024
Available online 26 January 2024

PO_4^{3-} (P_{ex}) is sufficient because diatom has a greater advantage in PO_4^{3-} affinity, and the growth demand for PO_4^{3-} is also higher. Therefore, the growth of diatom algal blooms quickly collapses after P_{ex} depletion (Ou et al., 2008). Dinoflagellates blooms such as *P. donghaiense* blooms have been observed in the coastal waters of the ECS from late April to June after diatom blooms when P_{ex} is insufficient because *P. donghaiense* has lower thresholds of PO_4^{3-} and could make good use of the metabolized dissolved organic phosphate or phagocytose the organic debris (Yu et al., 2017; Ou et al., 2008). This can be verified in the research by Lu and Li (2006), where the authors obtained that the luxury coefficient of PO_4^{3-} ($R_P = Q_{max}/Q_{min}$, 4.3, Q_{max} and Q_{min} are the maximum and minimum cell quota of P_i, respectively.) of *P. donghaiense* was higher than that of *S. costatum* (2.5), and its growth potential of storage P_i ($t_P = \ln R_P/\mu_{max}$, 2.08 day, μ_{max} is the maximum growth rate of algae.) was higher than that of *S. costatum* (0.53 day). This also indicates that phosphorus is a nutrient limiting phytoplankton biomass, which plays an important role in the long-lasting spring bloom of *P. donghaiense* in the ECS and YRE (Yu et al., 2017; Shen et al., 2019). Thus, by studying the uptake of PO_4^{3-} by algae, we can find an effective way to control algal bloom formation and biomass accumulation (Schindler et al., 2008; Kilham and Hecky, 1988).

The previous studies on PO_4^{3-} uptake by algae commonly focus on various culture environments such as P_{ex} concentration, illumination intensity, flowing rate, and temperature (Shi et al., 2015; Shen et al., 2016), and partition the growth of algae, especially in bloom, into four phases: slowly-growing, exponentially-growing, stable, and dissipation phases (Tester and Steidinger, 1997). During the growth of algae, fluctuations in both cell density and cell quota are frequently observed. This oscillatory behavior is a ubiquitous phenomenon in nature and can be found in diverse systems, such as aquatic ecosystems, predator–prey interactions, nervous systems, and epidemiological dynamics (Esmaeili et al., 2022; Huisman et al., 2006; Shen et al., 2023). In a field survey covering the process of a *P. donghaiense* bloom in the coastal waters of ECS from 9 to 20 May 2016, Shen et al. (2019) observed the oscillation phenomenon in the cell density of *P. donghaiense*. Several scholars have investigated the fluctuation of algae density through mathematical modeling. In a study by Song et al. (2019), a stoichiometric model was employed to examine the impact of seasonal light intensity and nutrient availability on algal fluctuations during algal blooms in the Bohai Sea. Building upon the model proposed by Song et al. (2019), Zhao et al. (2020) developed a stochastic growth model for algae, taking into account the influence of environmental randomness, and obtained the threshold conditions that determine the persistence and extinction of algae. Using actual photochemical quantum yield and cell density as research variables, Shen et al. (2023) proposed an algae growth model including cell growth delay, and studied the interaction between cell density and photosynthetic parameters during the fluctuating growth of algae. Understanding the mechanism behind oscillations in the algal growth process is indeed crucial as it can offer valuable insights into the specific PO_4^{3-} demands and assimilation abilities of algae, which helps predict algal blooms more accurately (Droop, 1983). However, as far as we know, few studies paid attention to the oscillations of cell density and cell quota appearing during the algae culture (Caperon, 1969; Cunningham and Maas, 1978; Droop, 1983; Muhammadu et al., 2017).

It has been observed that various algae species, including cyanobacteria, diatoms, and dinoflagellates, in different environments ranging from freshwater to the ocean, have the ability to passively adsorb and store inorganic phosphate (PO_4^{3-}) in their cell membrane or extracellular polymeric substances (EPS) (Sañudo-Wilhelmy et al., 2004; Xing et al., 2021; Zhang et al., 2013; Duan et al., 2023; Kamennaya et al., 2020; Zubkov et al., 2015). Most EPS-associated PO_4^{3-} can act as a nutrient buffer to support algal cell/aggregate growth (Duan et al., 2023). Duan et al. (2023) demonstrated that the enrichment of PO_4^{3-} in EPS increased the PO_4^{3-} content in cyanobacteria, leading to a prolonged maintenance of higher PO_4^{3-} concentrations and making it more challenging to mitigate algal blooms. Zubkov et al. (2015) showed that both *Prochlorococcus* and SAR11 cells possess an extracellular buffer of labile phosphate, which facilitates their survival in apparently P_{ex}-deficient waters. Zhang et al. (2013) indicated that EPS can serve as a dynamic storage of PO_4^{3-}, and its significant PO_4^{3-} accumulation capacity contributes to the PO_4^{3-} removal process in enhanced biological phosphorus removal. Additionally, Sañudo-Wilhelmy et al. (2004) suggested that the adsorption of PO_4^{3-} on the cell surface is part of the PO_4^{3-} uptake process. Thus, in the modeling of PO_4^{3-} uptake kinetics, distinguishing between the P_s pool and the P_i pool can provide a more accurate reflection of the PO_4^{3-} uptake characteristics of phytoplankton (Yao et al., 2011; Jiang et al., 2019; Gao et al., 2022).

In addition, it is important to consider the time delay, in the transport process from the P_s pool to the P_i pool when studying the PO_4^{3-} uptake mechanism in algal cells (Fu et al., 2006; Kamennaya et al., 2020). Kamennaya et al. (2020) showed that some bacteria and algae (such as SAR11, *Synechococcus*, and *Prochlorococcus*) possess a periplasmic space between the inner membrane and the outer membrane, which temporarily stores transported PO_4^{3-} from the cell surface. Subsequently, PO_4^{3-} is transported into the cytoplasm through ABC-type transporters (PstCAB) to support cell growth and reproduction (Kamennaya et al., 2020). This may lead to a time lag in the transport process of PO_4^{3-} from the P_s pool to P_i pool which has been well confirmed in literatures. For example, there is an obvious decoupling phenomenon between the rate of accumulation PO_4^{3-} in the periplasm and the growth rate in *Synechococcus*. A cultured *Synechococcus* cell can double the PO_4^{3-} of periplasmic within merely 3 h under the P_{ex} condition of 10^{-6} mol L^{-1}, while they divide every 1–2 days (Kamennaya et al., 2020). Similarly, *Prochlorococcus* and SAR11 cells can store enough PO_4^{3-} for cell division in only 1-2 h in the periplasm, whereas *Prochlorococcus* divides every 3.5 days (Zubkov, 2014) and SAR11 divides every 2–3 days (Mary et al., 2008) in oligotrophic waters.

In this study, we present a novel two-stage PO_4^{3-} uptake model that incorporates the transport time delay between the P_s pool and the P_i pool. Subsequently, the model is calibrated and validated using experimental data of *P. donghaiense* and *Karenia mikimotoi* under conditions of sufficient P_{ex} at temperature of 20 °C. By integrating the experimental and mathematical findings, we propose a possible plausible physiological mechanism that can account for the oscillations observed in algal cell quota. Additionally, we deeply discuss the ratio between P_i and the total cellular PO_4^{3-} which is crucial in understanding the specific PO_4^{3-} uptake process of algae. The exploration performed in this paper contributes to a comprehensive understanding of algal dynamics and has potential implications for the accurate prediction of HABs.

2. Materials and methods

2.1. Model description

In view of the presence of P_s pool, the process of PO_4^{3-} uptake by algae should be divided into two stages (Kamennaya et al., 2020; Duan et al., 2023; Yao et al., 2011; Jiang et al., 2019). Firstly, PO_4^{3-} in the substrate is passively adsorbed to the cell surface and stored in the P_s pool (Kamennaya et al., 2020; Duan et al., 2023). Secondly, surface-adsorbed PO_4^{3-} enters the cytoplasm through the translocator and then is assimilated to form newborn algal cells (Kamennaya et al., 2020; Solovchenko et al., 2019; Lin et al., 2016). The schematic diagram of the PO_4^{3-} uptake process in algal cells is shown in Fig. 1.

In this paper, A (10^8 cells L^{-1}) represents the density of algal cell and P (μmol L^{-1}) represents the concentration of P_{ex}. S (10^{-8}μmol $cell^{-1}$) and Q (10^{-8}μmol $cell^{-1}$) represent the cell quota of P_s and P_i, respectively. In the early phosphate uptake model proposed by Droop (1973), it is assumed that the algal specific growth rate (μ) is a function of the cell quota of P_i

$$\mu = \mu_{max}\left(1 - \frac{Q_{min}}{Q}\right), \tag{1}$$

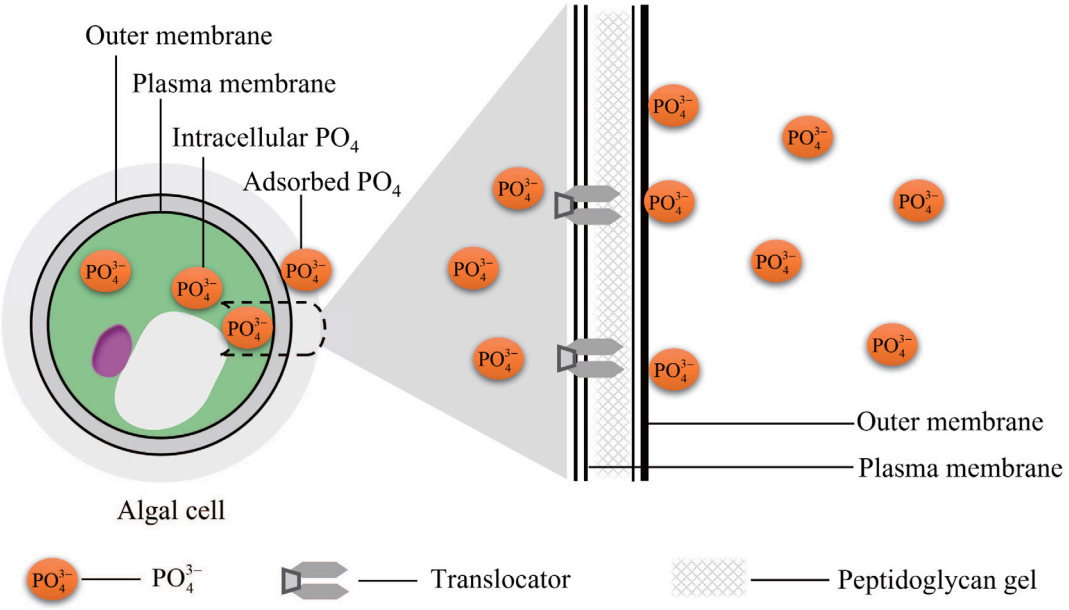

Fig. 1. Schematic diagram of the PO_4^{3-} uptake process in algal cells. First, PO_4^{3-} is passively adsorbed to the cell surface, and then transported into the cytoplasm by the translocator. *Source:* The conceptual diagram of the PO_4^{3-} uptake process in algae is adapted from Kamennaya et al. (2020).

where μ_{max} is the maximum growth rate of algae, Q_{min} is the minimum cell quota of P_i. Empirical evidences show that the Droop form describes data more accurately than the Monod form (Wang et al., 2022). Under fixed light intensity, the self-shading among algal cells will limit its growth rate with the increase of algal cell density. Therefore, the algal specific growth rate can be rewritten as

$$\mu = \mu_{max}\left(1 - \frac{Q_{min}}{Q}\right)\left(1 - \frac{A}{K}\right), \tag{2}$$

where K is the carrying capacity that depends on external factors bounding algae density (e.g. light and nutrients). The loss rate of algal cells due to natural mortality is assumed to be proportional to its density and determined by the death rate e. So the change rate of A can be expressed as

$$\frac{dA}{dt} = \mu A - eA. \tag{3}$$

The PO_4^{3-} adsorption rate of algal cells is proportional to the concentration of PO_4^{3-} in the environment. In addition, the adsorption rate is controlled by the concentration of PO_4^{3-} in the P_s pool. With the filling of the P_s pool, the adsorption rate decreases, when the P_s pool is full, the adsorption rate becomes zero (Zubkov et al., 2015). Based on these assumptions, the PO_4^{3-} adsorption rate R_a can be described by the following function,

$$R_a = K_a S\left(1 - \frac{S}{S_{max}}\right)\frac{P}{P + K_p}, \tag{4}$$

where K_a is the adsorption rate, S_{max} is the maximum cell quota of P_s, K_p is the half-saturation coefficient of algal nutrient adsorption. Note that the PO_4^{3-} adsorption process by algal cells is reversible, P_s can be desorbed into the substrate with a rate of K_d (Zhou et al., 2017a; Yao et al., 2011).

Generally, the PO_4^{3-} transport process of algal cells through specialized transporters located in the cell membrane, and the type and abundance of these transporters have a profound effect on the PO_4^{3-} transport (Solovchenko et al., 2019). In addition, the surface-adsorbed PO_4^{3-} concentration has an important impact on the transport rate. The higher the surface-adsorbed PO_4^{3-}, the more readily it can be bound with transporters to increase the transport rate of PO_4^{3-} (Lin et al., 2016; Zubkov et al., 2015; Kamennaya et al., 2020). As the external environment undergoes changes, the demand for PO_4^{3-} by algal cells may also vary. To effectively utilize the variability in this supply–demand relationship within cells, it is necessary to coordinate a cellular feedback system. This system should be able to sense both the cell surface PO_4^{3-} pool and the intracellular PO_4^{3-} pool, and adjust the number of cellular PO_4^{3-} transporters and enzymes that utilize dissolved organic phosphorus (DOP) in a rational manner (Lin et al., 2016). Therefore, the PO_4^{3-} transport process is co-regulated by the P_i pool and the P_s pool. The PO_4^{3-} transport rate T can be described by the following function,

$$T = \gamma F(Q) S, \tag{5}$$

where γ is the maximum PO_4^{3-} transport rate of algae. $F(Q)$ is a feedback function that describes the influence of the P_i pool on PO_4^{3-} transport. Feedback is a fundamental characteristic of biochemistry, enabling organisms to regulate their growth and interactions with physicochemical processes. This mechanism is often represented using a simple Michaelis–Menten function, which relates concentration to rate (Flynn et al., 1997). However, employing the Michaelis–Menten function to regulate the course of the PO_4^{3-} pool changes can result in excessively rapid rate changes, leading to the P_i pool being nearly empty or completely full. In reality, these relationships can be more accurately described by a sigmoidal (Hill) function with a power of 4, which aligns with the allosteric nature of enzymatic processes (Flynn et al., 1997). The efficacy of using a sigmoidal function with a power of 4 to depict the feedback of algal cells on PO_4^{3-} transport has also been demonstrated in several other studies (Yao et al., 2011; John and Flynn, 2000; Gao et al., 2022; Jiang et al., 2019). Following the same logic, in this paper, we use the following sigmoidal function to express the feedback of the P_i pool on PO_4^{3-} transport,

$$F(Q) = \frac{\left(1 - \frac{Q}{Q_{max}}\right)^4}{\left(1 - \frac{Q}{Q_{max}}\right)^4 + K_q}, \tag{6}$$

where Q_{max} and K_q are the maximum cell quota of P_i and the constant in the feedback function, respectively.

Furthermore, since PO_4^{3-} can be stored transiently in the periplasm, which may introduce a time delay, denoted by τ, in the transport of PO_4^{3-} from the cell surface to the cell interior (Kamennaya et al., 2020; Zubkov et al., 2015). Several literatures have reported that there

Table 1
Parameters in model (10).

Parameter	Units	Explanation
μ_{max}	day^{-1}	Maximum specific growth rate of algae
Q_{min}	μmol $cell^{-1}$	Minimum cell quota of intracellular PO_4^{3-}
K	cells L^{-1}	Resource carrying capacity determined by nutrient and light
e	day^{-1}	Death rate of algae
γ	day^{-1}	Maximum PO_4^{3-} transport rate of algae
τ	day	Time lag for the transport of PO_4^{3-} from the P_s pool to the P_i pool
Q_{max}	μmol $cell^{-1}$	Maximum cell quota of intracellular PO_4^{3-}
K_q		Constant in the feedback function
K_a	day^{-1}	Adsorption rate
K_d	day^{-1}	Desorption rate
S_{max}	μmol $cell^{-1}$	Maximum cell quota of surface-adsorbed PO_4^{3-}
K_p	μmol L^{-1}	Half-saturation coefficient of algal nutrient adsorption
r		Decomposition ratio of dead algal cells

is a time lag of several days between the accumulation of PO_4^{3-} in the algal periplasm and the growth of the algae (Kamennaya et al., 2020; Zubkov, 2014; Mary et al., 2008). Therefore, it is reasonable and necessary to consider the time lag in modeling the transport of PO_4^{3-} from the cell surface to the cell interior. It is worth noting that the transport process of PO_4^{3-} is regulated by both the P_i pool and the P_s pool. As a result, the transport rate of PO_4^{3-} at a given time t is influenced by the concentrations of both intracellular PO_4^{3-} and cell surface PO_4^{3-} at a previous time $t-\tau$. Consequently, at time t, the final form of PO_4^{3-} transport rate per algal cell can be rewritten as

$$T_\tau = \gamma \frac{\left(1-\frac{Q_\tau}{Q_{max}}\right)^4}{\left(1-\frac{Q_\tau}{Q_{max}}\right)^4 + K_q} S_\tau, \tag{7}$$

where the notation Q_τ means $Q(t-\tau)$.

During the growth and division of algal cells, the PO_4^{3-} cell quota undergoes simultaneous dilution. It is important to note that this dilution process is synchronized with the growth of the algal cells, and the dilution rate of the PO_4^{3-} quota is equal to the specific growth rate μ (Wang et al., 2007; Yan et al., 2022; Bonachela et al., 2011). In summary, the rate of change of Q and S at time t can be expressed as

$$\begin{aligned} \frac{dQ}{dt} &= T_\tau - \mu Q, \\ \frac{dS}{dt} &= R_a - K_d S - T - \mu S. \end{aligned} \tag{8}$$

For dead algal cells, we assume that part of them can be decomposed and the PO_4^{3-} in the P_i pool and the P_s pool can be released into the substrate for recycling (Wang et al., 2008; Tiwari et al., 2017). Therefore, the change rate of P at time t can be expressed as

$$\frac{dP}{dt} = reA(Q+S) - R_a A + K_d AS, \tag{9}$$

where r is the decomposition ratio of dead algal cells.

Based on the above arguments, we obtain the following novel PO_4^{3-} uptake model,

$$\frac{dA}{dt} = \underbrace{\underbrace{\mu_{max}\left(1-\frac{Q_{min}}{Q}\right)\left(1-\frac{A}{K}\right)}_{\mu\text{: specific growth rate}} A}_{\text{cell growth}} - \underbrace{eA}_{\text{cell death}}, \tag{10a}$$

$$\frac{dQ}{dt} = \underbrace{\gamma S_\tau \frac{\left(1-\frac{Q_\tau}{Q_{max}}\right)^4}{\left(1-\frac{Q_\tau}{Q_{max}}\right)^4 + K_q}}_{F\text{: delayed feedback function}} - \underbrace{\mu_{max}\left(1-\frac{Q_{min}}{Q}\right)\left(1-\frac{A}{K}\right) Q}_{\mu\text{: dilution rate}}, \tag{10b}$$

$$\frac{dS}{dt} = \underbrace{K_a S\left(1-\frac{S}{S_{max}}\right)\frac{P}{P+K_p}}_{R_a\text{: } PO_4^{3-} \text{ adsorbed from substrate}} - \underbrace{K_d S}_{\text{desorption}}$$

$$- \underbrace{\frac{\left(1-\frac{Q}{Q_{max}}\right)^4}{\left(1-\frac{Q}{Q_{max}}\right)^4 + K_q} S}_{T\text{: } PO_4^{3-} \text{ transport rate}} - \underbrace{\mu_{max}\left(1-\frac{Q_{min}}{Q}\right)\left(1-\frac{A}{K}\right) S}_{\text{dilution due to cell division}}, \tag{10c}$$

$$\frac{dP}{dt} = \underbrace{reA(Q+S)}_{PO_4^{3-} \text{ recycling from dead algal cells}} - \underbrace{K_a S\left(1-\frac{S}{S_{max}}\right)\frac{P}{P+K_p} A}_{\text{adsorbed by algal cells}} + K_d SA. \tag{10d}$$

The biological meanings and units of parameters are listed in Table 1.

2.2. Materials and methods

2.2.1. Algal culture conditions

Prorocentrum donghaiense was provided by Douding Lu of the Second Institute of Oceanography, Ministry of Natural Resources of the People's Republic of China (MNR) in Hangzhou, China. These algal cells were pre-cultured at 20 °C in f/2 medium (Guillard, 1975). The light intensity and light : dark cycle of these cultures were 65-70 μmol photons m^{-2} s^{-1} and 12:12 h, respectively. All cultures were performed in an illumination incubator. The cultures were shaken vigorously twice times daily within the set time in case the algal cells gathered at the bottom. The algal cells used in the following experiments were those cultured to exponential growth phase.

2.2.2. Phosphate uptake experiments

The initial cell density of these batch cultures was about 0.15×10^8 cells L^{-1}, and the initial P_{ex} concentration is 35.08 μM. Three biological repeats were used in the P_i uptake experiments. A 10 mL sample was collected every 3 days (0, 3, 6, 9, 12, 15, 18, 21, 24, 27, and 30 day). The detection methods for P_{ex}, P_s, and P_i, based on Yao et al. (2011), were used with minor modifications. Specifically, each sample was immediately filtered through a 0.22 μm cellulose acetate membrane after sampling to analyze the P_{ex} concentration in the filtrate using phosphomolybdate-blue spectrophotometry. Then, the membrane containing microalgal cells was thoroughly washed with 10 mL of oxalic acid reagent, followed by filtration through a 0.22 μm cellulose acetate membrane to analyze the filtrate using phosphomolybdate-blue spectrophotometry for P_s. The microalgal cells remaining on the membrane were washed out using 10 mL of MQ water, digested using the potassium persulfate method, and analyzed with phosphomolybdate-blue spectrophotometry for P_i. To monitor the growth of microalgae, a 0.5 mL sample was taken and preserved in Lugol's solution for direct cell density (A) counting, while 0.1 mL samples were counted using a phytoplankton counter frame (CC-F, Beijing purity instrument, Co., Ltd., China) and an optical microscope (BX43, Olympus, Japan) at day 0, 3, 6, 9, 12, 15, 18, 21, 24, 27, and 30.

2.3. Statistical analysis

The experimental data are presented as the mean ± SE of triplicates, which follows the normal distribution with homogeneous variance (Levene tests). One-way ANOVA and Tukeys multiple range test were used to analyze the statistical differences between sample days. p values < 0.05 were considered statistically significant. All analyses were performed using IBM SPSS Statistics 22.0 (IBM SPSS Software, Chicago, USA), and all pictures are drawn by MATLAB (R2016b).

2.4. Model calibration and validation

Based on the experimental data of *P. donghaiense*, the parameter values of model (10) are estimated by the least square method. This process is implemented by the "fmincon" function of MATLAB (R2016b). The following objective function is used in this study,

$$f(\Phi, m) = \frac{1}{m}\sum_{i=1}^{m} cost_i,$$

where Φ is a vector of parameters to be calibrated, m is the number of model variables used for model calibration at the same time. $cost_i$ is the model cost of the ith state variable (Adhurya et al., 2021; Gao et al., 2022),

$$cost_i = \sum_{j=1}^{n} \frac{(X_{ij}^{sim} - X_{ij}^{obs})^2}{(X_{ij}^{obs})^2},$$

where n is the number of observed values of a variable, X_{ij}^{sim} and X_{ij}^{obs} are respectively the simulation value and the observed value of the ith state variable at day j. The model cost provides a measure of the overall fit of the model to the data. In addition, we also calculate the relative error of all model variables. The relative error expresses the difference between the predicted and observed values as a percentage of the observed value. The relative error of the ith state variable of model is calculated by the below equation (Marois and Mitsch, 2016):

$$RE_i = \frac{1}{n}\sum_{j=1}^{n}\left(\frac{X_{ij}^{sim}}{X_{ij}^{obs}} - 1\right) \times 100.$$

By calculating the costs and relative errors for all model variables, we can assess the accuracy and goodness of fit of model (10) to the experimental data.

3. Results

3.1. Experimental data and fitting results

The model fitting results and experimental data of the state variables of A, P, Q and S of *P. donghaiense* at 20 °C under P_{ex}-sufficient condition are shown in Fig. 2. The estimated parameter values are listed in Table 2. Table 3 shows the model cost and relative error for each state variable of model (10) during the calibration and validation. The tendency of each state variable for given initial value can be observed in Fig. 2. Specially, with the initial 0.15×10^8 cells L^{-1}, A declined in the first 3 days, increased slowly in the next 6 days and then increased significantly ($p < 0.05$) from day 9 to day 15 and reached a peak value on day 15, finally reached another peak value on day 27. With the initial P_{ex} concentration in substrate 35.08 μM, P decreased throughout the experiment, rapidly in the first 20 days and slowly in the last 10 days. With the initial 9.43×10^{-8} μmol $cell^{-1}$, Q showed a significant trend of fluctuation ($p < 0.05$), and the fluctuation range was gradually decreasing. With the initial 13.53×10^{-8} μmol $cell^{-1}$, S showed a downward fluctuation trend during the experiment, and the fluctuation range was also gradually decreasing. In detail, S increased significantly ($p < 0.05$) in the first 3 days, obtained a maximum value of 24.57×10^{-8} μmol $cell^{-1}$ on day 3, decreased fast in the next 9 days, and then emerged the phenomenon of oscillation in the last 18 days.

Table 2
Parameter values of model (10) estimated from experimental data of A, Q, S and P in *P. donghaiense*.

Parameter	Unit	Value
μ_{max}	day^{-1}	0.52
Q_{min}	μmol $cell^{-1}$	3.8×10^{-8}
K	cells L^{-1}	2.8×10^{8}
e	day^{-1}	0.175
γ	day^{-1}	2.23
Q_{max}	μmol $cell^{-1}$	18.8×10^{-8}
τ	day	3.05
K_q		0.23
K_a	day^{-1}	1.92
K_d	day^{-1}	0.28
K_p	μmol L^{-1}	14.3
S_{max}	μmol $cell^{-1}$	39.5×10^{-8}
r		0.92

Table 3
Model costs and relative errors for all variables.

State variable	Model cost	Relative error
A	1.54	10.24
Q	0.45	10.43
S	6.64	24.95
P	0.48	7.61
$P_i/(P_i + P_s)$	0.45	1.97

Combining model cost and relative error, it can be seen from Fig. 2, Q has the best simulation effect among the four variables, with the smallest model cost 0.45. The cell density of algae (A) and the substrate PO_4^{3-} concentration (P) also fit well and the relative errors are 1.53 and 0.48, respectively. For S, the simulated curve is basically consistent with the experimental data, especially the first peak (day 3) and the last 12 days. But, from day 12 to day 15, the fitted curve of model (10) significantly deviates from the experimental data. This discrepancy may be attributed to the ability of algal cells to synthesize and store PolyP (Solovchenko et al., 2019; Jin et al., 2021; Lin et al., 2016). The presence of PolyP can enhance the uptake of PO_4^{3-} by algal cells, leading to a prolonged decrease in P_s. However, our model only accounts for the transport process of PO_4^{3-} from the cell surface to intracellular. Consequently, this limitation may result in inconsistencies between the solution of model (10) and the experimental data. It is important to mention that we also conduct simulations using the no-delay model with the parameter values in Table 2. The results are presented in Fig. 2. It is evident that both the model with time delay and the model without time delay yield similar fitting results for the experimental data of A and P. However, when considering the cell quota data (Q and S), a noticeable discrepancy in the fitting results emerges. The model with time delay demonstrates a satisfactory fit to the experimental data, while the model without time delay fails to adequately capture the data. These simulation results provide compelling evidence that the time delay in the transport of PO_4^{3-} from the cell surface to the cell interior may serve as a physiological mechanism leading to the oscillations in the cell quota.

Furthermore, we compare the solutions of model (10) with the experimental data of the ratio of intracellular PO_4^{3-} to total cellular PO_4^{3-} ($P_i/(P_i + P_s)$). The parameter values are from Table 2, and the initial values of A, P, Q, and S are 0.15×10^8, 35.08, 9.43×10^{-8}, and 13.53×10^{-8}, respectively. The result presents in Fig. 3 shows a strong agreement between the solution and experimental data. The model accurately captures the changing trend observed in experimental data. The model cost is 0.45 and the relative error is 1.97. In contrast, the model without delay fails to capture the observed trends in the experimental data.

Finally, model (10) is validated using experimental data of *K. mikimotoi* under conditions of sufficient extracellular PO_4^{3-} at temperature of 20 °C. The initial values of A, P, Q, S, are 0.2×10^8, 25.56,

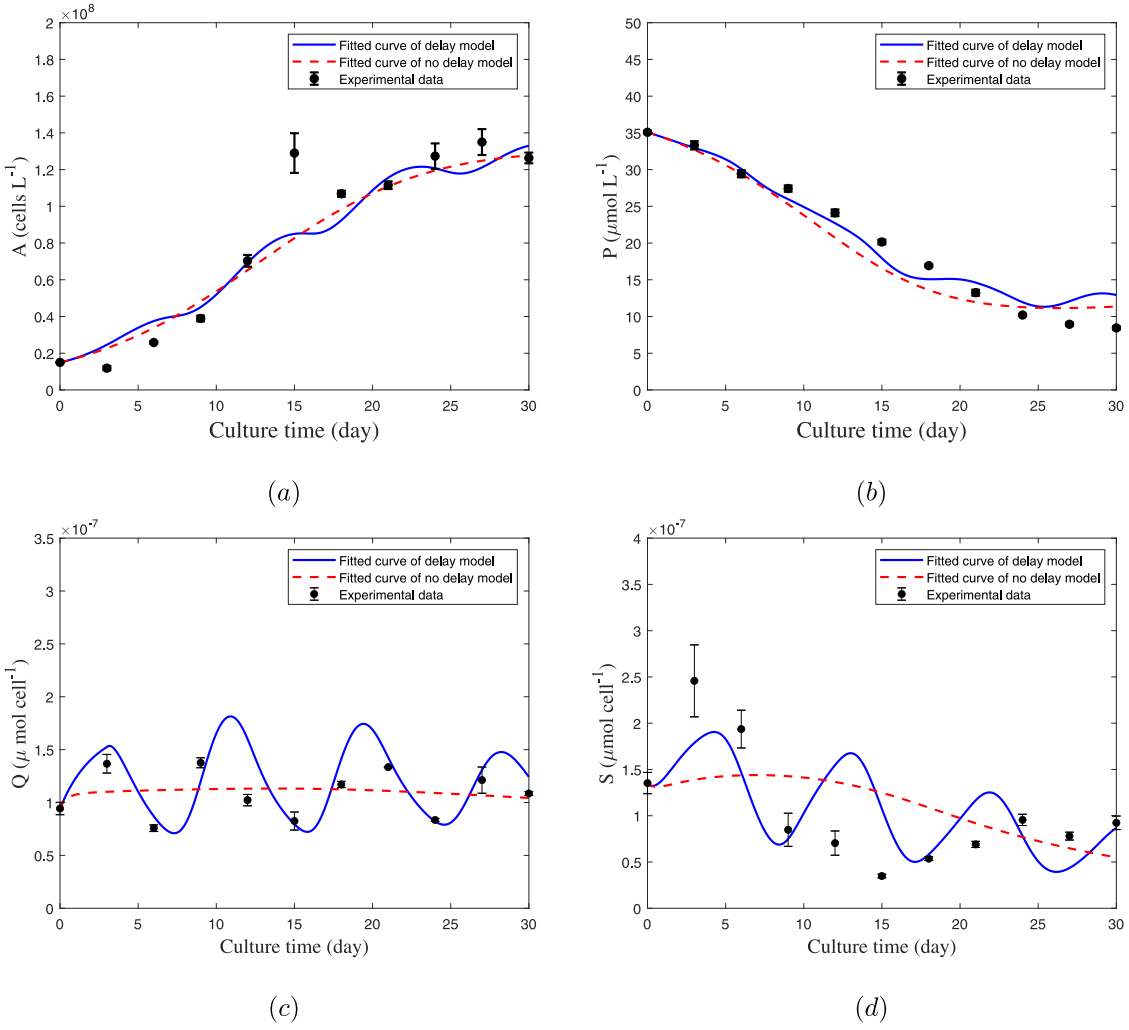

Fig. 2. Comparison of the fitted curves of the delay model (shown as a blue solid line) and the no-delay model (shown as a red dash line) with the experimental data of *P. donghaiense* at 20 °C under P_{ex} sufficient condition. (a) cell density (A); (b) Concentration of P_{ex} (P); (c) the cell quota of P_i (Q); (d) the cell quota of P_s (S). The parameter values of model (10) can be estimated by fitting the four state variables simultaneously, and the values are shown in Table 2. The experimental data is expressed as mean ± SE.

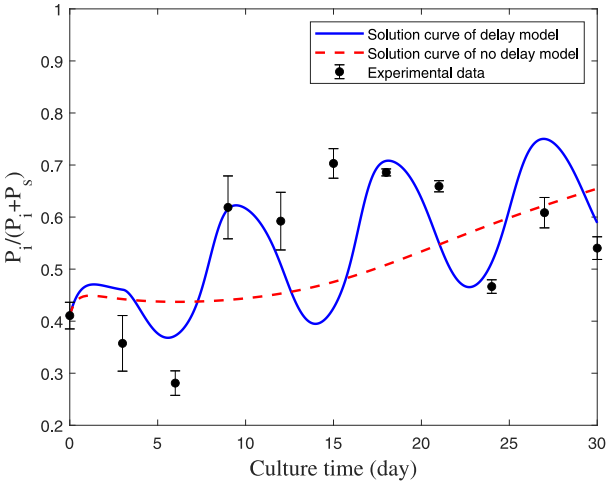

Fig. 3. The comparison of model (10) with experimental data of $P_i/(P_i+P_s)$ (the ratio of P_i to the total cellular PO_4^{3-}). The blue solid line represents the solution curve of the delay model, while the red dash line represents the no-delay model. The parameter values from Table 2. The experimental data is expressed as mean ± SE.

6.7×10^{-8}, and 19.69×10^{-8}, respectively. The validation results are shown in Fig. 4. The parameter values used in the validation are as follows: $K_a = 4.18$, $K_q = 3.12$, $K_n = 0.5$, $e = 0.245$, $r = 0.7$, $K = 16.8\times10^8$, $Q_{\max} = 38.32 \times 10^{-8}$, $Q_{\min} = 0.92 \times 10^{-8}$, and $S_{\max} = 24.83 \times 10^{-8}$, where the values of $Q_{\max}$, $Q_{\min}$, and $S_{\max}$ are from Gao et al. (2022). The remaining parameter values utilized in the model are obtained from Table 2. The validation results show that our model accurately captures the PO_4^{3-} uptake characteristics of *K. mikimotoi* with appropriate parameter values (Fig. 4). The calibration and validation results provide strong evidence that the two-stage PO_4^{3-} uptake model with transport delay effectively describes the PO_4^{3-} uptake characteristics of *P. donghaiense* and *K. mikimotoi* under the conditions of P_{ex}-sufficient at 20 °C.

3.2. Sensitivity analysis

To gain a comprehensive understanding of the influence of different input parameter values and their variations on the model results, a sensitivity analysis is conducted for all variables in model (10) with respect to several important model parameters. This analysis aim to assess how changes in these parameters affect the model solutions and provide insights into their relative importance in determining the model outcomes. These parameters are the maximum specific growth rate of algal cells ($\mu_{\max}$), the maximum cell quota of surface-adsorbed

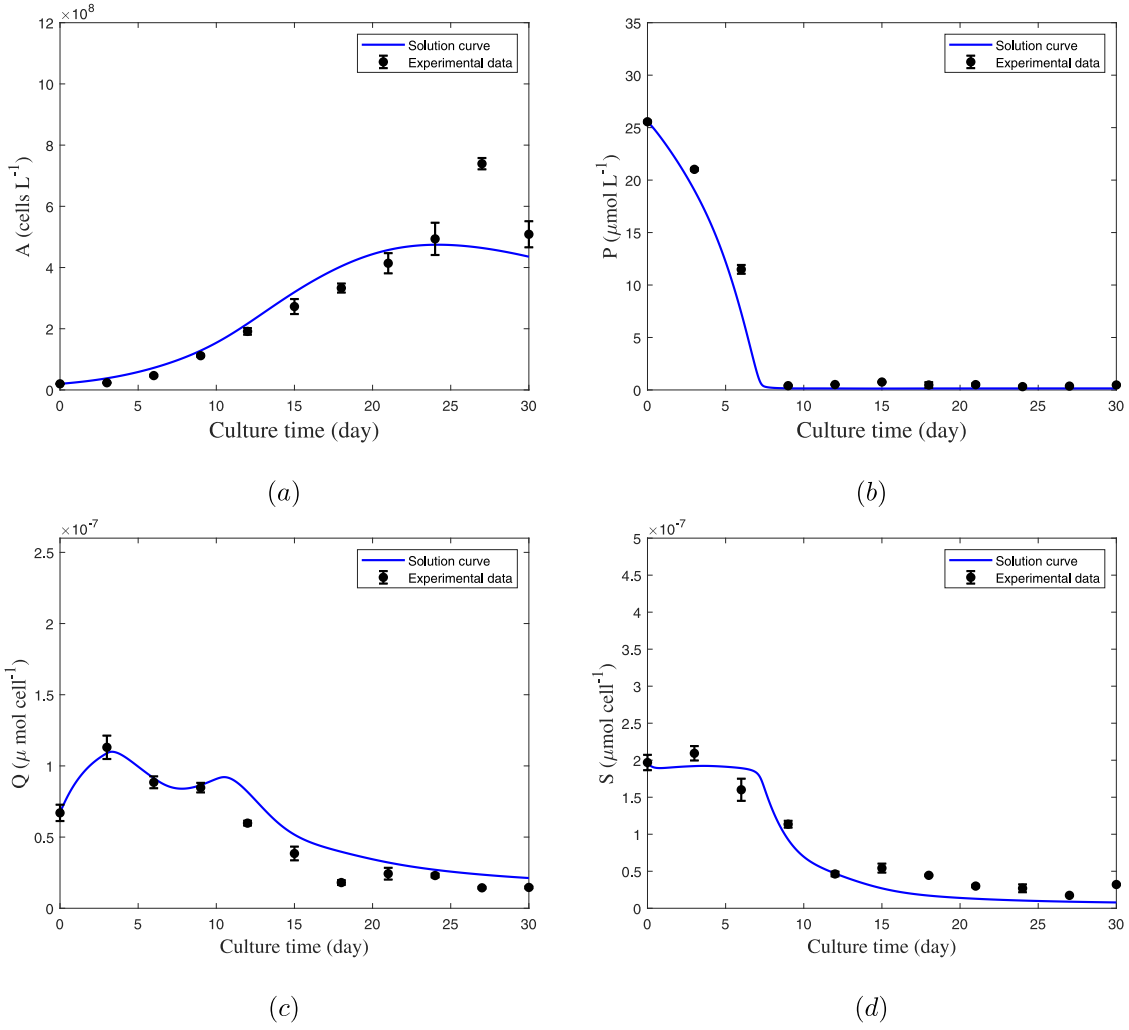

Fig. 4. The validation of model (10) is performed using experimental data of *Karenia mikimotoi* under the condition of sufficient P_{ex} at 20 °C. The parameter values used in the validation are as follows: $K_a = 4.18$, $K_q = 3.12$, $K_n = 0.5$, $e = 0.245$, $r = 0.7$, and $K = 16.8 \times 10^8$. The values of $Q_{max} = 38.32 \times 10^{-8}$, $Q_{min} = 0.92 \times 10^{-8}$, and $S_{max} = 24.83 \times 10^{-8}$ of *Karenia mikimotoi* are obtained from Gao et al. (2022). The remaining parameter values are listed in Table 2. The experimental data is expressed as mean ± SE.

PO_4^{3-} (S_{max}), the minimum cell quota of P_i (Q_{min}), the adsorption rate of PO_4^{3-} on cell surface (K_a), the time lag for the transport of PO_4^{3-} from the P_s pool to the P_i pool (τ), the decomposition ratio of dead algal cells (r), the maximum cell quota of intracellular PO_4^{3-} (Q_{max}), the maximum PO_4^{3-} transport rate of algae (γ), respectively. The baseline values of parameter are from Table 2. For this purpose, we derive the sensitivity system of the partial derivative of the variable $X = \{A, P, Q, S\}$ of model (10) with respect to the parameters $q = \{\mu_{max}, S_{max}, Q_{min}, K_a, \tau, r, Q_{max}, \gamma\}$ (the detail methods please see Bortz and Nelson (2004), Shen et al. (2023)).

The semi-relative sensitivity solutions ($q\frac{\partial X}{\partial q}$) for all state variables of model (10) are displayed in Fig. 5. It is important to clarify that the information presented in Fig. 5 does not represent the difference between the solutions in Fig. 2 and the solutions obtained from model (10) with slightly increased parameters. Instead, it provides a time series diagram showing the derivatives of the state variables with respect to the selected parameters. In addition, the logarithmic sensitivity curves ($\frac{\partial X}{\partial q}\frac{q}{X}$) for all state variables of model (10) are also calculated and displayed in Fig. 6. From the log-sensitivity solution curve, we can explain the percentage of solution change caused by positive perturbation of the parameter. As can be seen from Figs. 5 and 6, the semi-relative sensitivity solution and the logarithmic sensitivity solution have similar trends, but they represent different meanings.

From the sensitivity analysis results, we can observe that r has a positive effect on all variables of model (10), with a particularly significant impact on Q and S (Figs. 5 and 6). Although the effect of r is initially small, it gradually increases over time. This phenomenon may be due to the relatively high concentration of PO_4^{3-} in the medium at the early stage of the experiment, which is the main source of PO_4^{3-} for algae growth. As the algal population increases, the P_{ex} is heavily consumed, and the decomposition of cellular PO_4^{3-} from dead algal cells becomes a vital source of PO_4^{3-} for cell growth. Additionally, μ_{max}, K_a, Q_{max}, γ, and S_{max} have positive effects on algal cell density, while Q_{min} plays a negative role. Specifically, μ_{max} shows the most positive effect on cell density, while Q_{min} has the most significant negative effect (see Figs. 5a and 6a). μ_{max} is the maximum growth rate of algal cells, and its increase will obviously has a positive impact on cell density. Q_{min} is minimal P_i concentration to maintain cell growth, so its increase will lead to a decrease in cell density. Initially, these two parameters have minimal impact on cell density, but their influence gradually increases over time before ultimately decreasing. Notably, the effect of μ_{max} on cell density reaches its maximum value at day 20 (see Fig. 5a). Doubling μ_{max} at this time yields an approximate increase of 2.28×10^8 cells in density. After day 20, the effect of μ_{max} gradually decreases, possibly due to the growth rate of algae being primarily limited by light and resource availability during the final stages of the experiment. Moreover, as depicted in Fig. 6a, doubling μ_{max} and Q_{min} result in an increase of over 200% and a decrease of over 100% in algal density, respectively. The influences of K_a and S_{max} on P are negative, initially increasing and then decreasing over time.

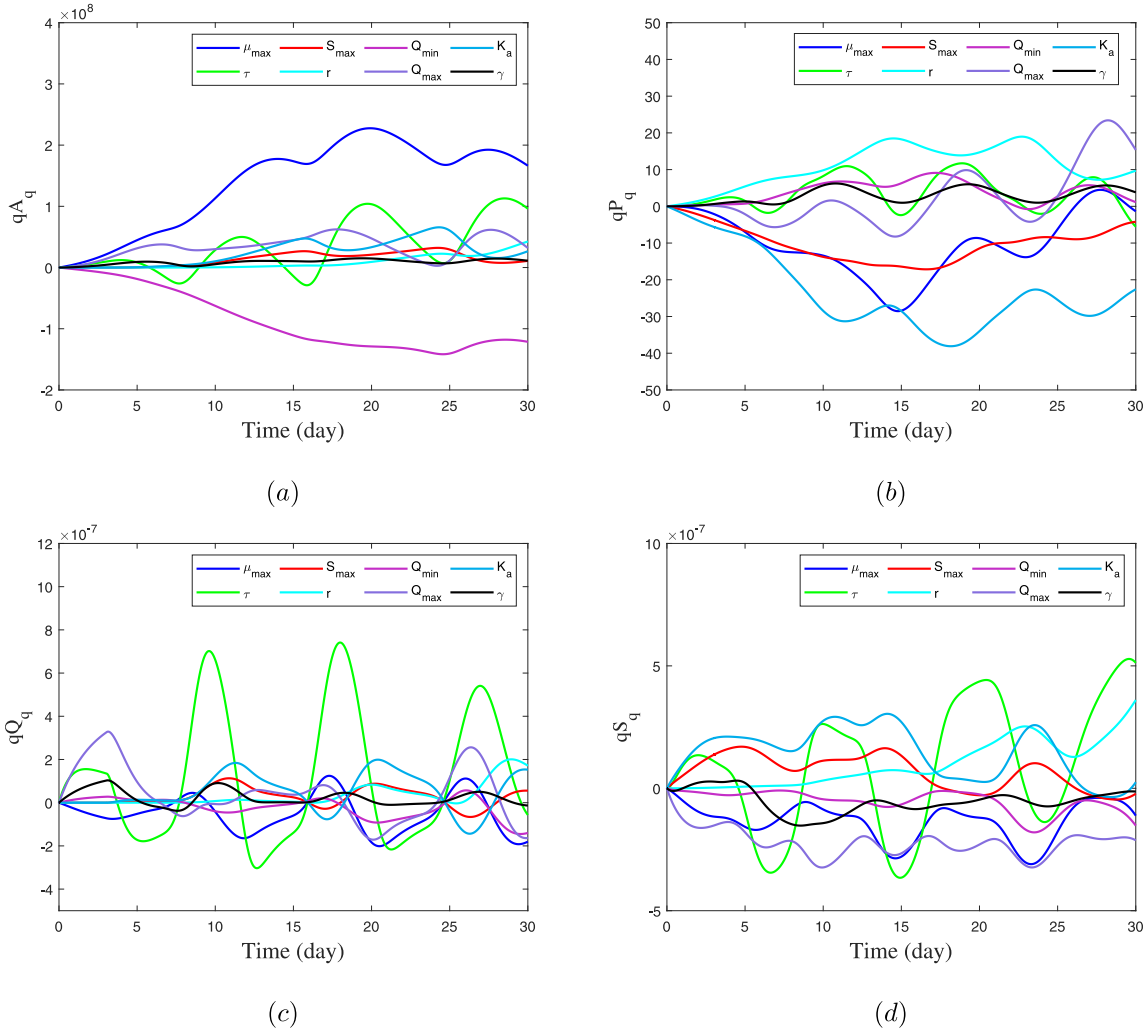

Fig. 5. The semi-relative sensitivity solutions ($q\frac{\partial X}{\partial q}$) for four variables of model (10), with respect to the important model parameters $q = \{\mu_{\max}, S_{\max}, Q_{\min}, K_a, \tau, r, Q_{\max}, \gamma\}$. Here the baseline values of parameter are shown in Table 2.

The effects of all parameters, except r, on Q are complex, with their influences fluctuating between positive and negative over time. This complexity may be caused by the time delay of PO_4^{3-} transport from the cell surface to the intracellular. Furthermore, $Q_{\min}$, $Q_{\max}$, and $\mu_{\max}$ play negative roles for S, whereas K_a and $S_{\max}$ exhibit positive effects in the initial stage and finally becoming negative. The impact of τ on all variables is intricate, with both positive and negative effects observed as time progresses. Moreover, the effects of τ on cell quota variables (S and Q) are significantly greater than its effects on cell density (A) and extracellular PO_4^{3-} concentration (P), the reason for which may be because τ describes the time lag of PO_4^{3-} transport from the surface of a single cell to the interior of the cell. These findings align with the simulation results obtained from models with and without time delay (see Fig. 2).

4. Discussion

In this paper, we develop a novel model based on the two-stage model of Jiang et al. (2019) by further incorporating the transport delay from P_s pool to P_i pool and the decomposition process of dead algal cells. The model is calibrated and validated by the experimental data of *P. donghaiense* and *K. mikimotoi* under P_{ex}-sufficient condition at 20 °C. The validity of model (10) con be confirmed from the intuitive fitting results, model cost, and relative error. In addition, we conduct a sensitivity analysis of the parameters, and the results are shown in Figs. 5 and 6. These results show that the maximum specific growth rate $\mu_{\max}$ is the most sensitive parameter for the density of algal cells, and the adsorption rate K_a has the most negative effect on P_{ex} concentration. The fitting results of model (10) to the experimental data and the validation results show that our model can better capture the phosphate uptake kinetics of algae through proper parameterization.

One notable highlight of our work is the introduction of the delay describing time spent in the transport process of from P_s pool to P_i pool. By comparing the fitting results of the delay model and the no-delay model, it can be found that the model with time delay can better fit experimental data, especially the changes of the surface-adsorbed PO_4^{3-} pool and intercellular PO_4^{3-} pool of algal cell can be well captured. Through parameter fitting, the estimated parameter value of time delay $\tau = 3.05$, which is consistent with previous research results (Kamennaya et al., 2020; Mary et al., 2008; Zubkov, 2014). The experimental and mathematical results provide convincing evidence that the time delay in the transfer of PO_4^{3-} from the P_s pool to the P_i pool may be a possible physiological mechanism leading to the oscillation of algal cell quota. Any delay arising from accumulated time constants may cause instability, as any control system may oscillate when there is a phase transition between the received and response information (Droop, 1983). Our results illustrate the significance of the time delay in influencing the PO_4^{3-} uptake kinetics of algae.

In addition, following the modeling ideas of Jiang et al. (2019) and Yao et al. (2011), the P_s pool and P_i pool are considered as two

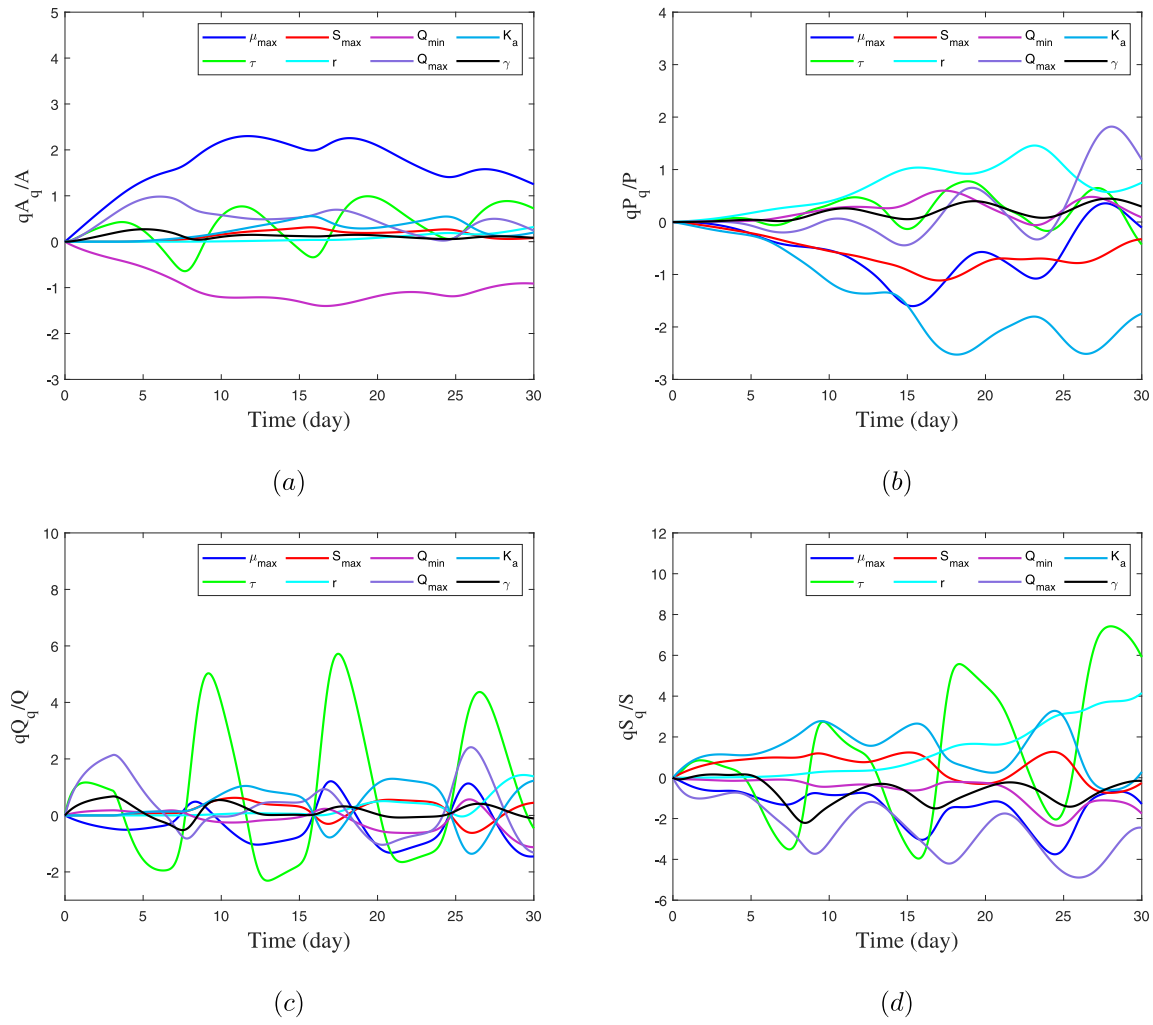

Fig. 6. The logarithmic sensitivity solutions ($\frac{\partial X}{\partial q}\frac{q}{X}$) for four variables of model (10), with respect to the important model parameters $q = \{\mu_{max}, S_{max}, Q_{min}, K_a, \tau, r, Q_{max}, \gamma\}$. Here the baseline values of parameter are shown in Table 2.

independent compartments in our model. Some studies have shown that P_s pool has a significant proportion of the total cellular PO_4^{3-} pool of algae. Our experimental results showed that the ratio range of P_s pool to the total PO_4^{3-} pool of *P.donghaiense* is 3 – 72% under P_{ex} sufficient condition, consistent with the previous reports. Qu et al. (2020) reported that the ratio of P_s pool to total cellular PO_4^{3-} pool of *P. donghaiense* could reach 9 – 72% in P_{ex} sufficient laboratory culture. The proportion of P_s pool on the cell surface of wild phytoplankton samples ranged from 7% to 36% in the Sanggou Bay (Xu and Liu, 2016), 15% to 46% in the Delaware Inland Bays and Delaware River Estuary (Fu et al., 2005), 0.7% to 34% in Lake Erie (Saxton et al., 2012), and 4% to 54% in the Yellow sea (Jin et al., 2021). Sañudo-Wilhelmy et al. (2004) indicated that the proportion of P_s in the senescent phase of *Thalassiosira weissflogii* could reach 90%, significantly higher than that in the exponential growth phase (30%). Fig. 3 shows that the solution curve of model (10) can well agree with the experimental data of $P_i/(P_i+P_s)$. In addition, the proportion of P_i to total PO_4^{3-} (P_i+P_s) shows a fluctuating trend during algae culture. The distribution of PO_4^{3-} between P_s pool and P_i pool is affected by many factors, such as growth stage, PO_4^{3-} demand of algal cell, and P_{ex} concentration (Fu et al., 2005). It can be seen from Figs. 2(a) and 3 that the ratio of P_i to the total cellular PO_4^{3-} is low in the early stage of the experiment while higher in the exponential growth and maintenance phase of the cells, which is consistent with the previous research results (Sañudo-Wilhelmy et al., 2004; Saxton et al., 2012; Jin et al., 2021). Thus, during the high-incidence season of algal blooms, once $P_i/(P_i+P_s)$ of some bloom-forming algae species exceeds a certain threshold, we can send out algal bloom warnings and take corresponding steps. Besides the relevance to cell growth, the plasticity of $P_i/(P_i+P_s)$ can also reflect the change in P_{ex} concentration. On the other hand, algal cells can adjust the level of intracellular P_i while maintaining a relatively stable growth rate for persistence across a range of P_i concentrations that do not allow for the accumulation of significant biomass (Saxton et al., 2012), which may lead to the oscillations of Q and S (Fig. 2). Thus, stoichiometry flexibility on total PO_4^{3-} partitioning plays an essential role in the growth of microalgae in environments where nutrients are highly variable, for example, large lakes and estuarine systems (Saxton et al., 2012; Davies and Wang, 2021; Wang et al., 2008; Yuan et al., 2020).

Notice that the study performed in this paper specifically focuses on examining the process of PO_4^{3-} uptake by algae under controlled laboratory conditions. In fact, algal cells can also respond to changes in light availability by modulating photosynthetic activity and growth rate, and therefore the alternating control of light and PO_4^{3-} may serve as a potential mechanism leading to the oscillation of algal cell density and cell quota. To provide more accurate descriptions of PO_4^{3-} assimilation mechanism and phytoplankton growth characteristics in a changing environment, the model proposed in this paper should be further enhanced by considering additional environmental factors such as solar irradiance, water velocity, environmental toxins, and the direct or indirect interactions among algal species (Yang and Yuan, 2021; Xu et al., 2021). We leave these for our future investigations.

CRediT authorship contribution statement

Anglu Shen: Conducted the experimental work, Data curation,Writing – original draft, Writing – review & editing, Funding acquisition. **Shufei Gao:** Data curation,Writing – original draft, Writing – review & editing. **Jie Jiang:** Data curation,Writing – original draft. **Qingjing Hu:** Writing – review & editing, Funding acquisition. **Hao Wang:** Conceptualization, Methodology, Writing – review & editing, Funding acquisition. **Sanling Yuan:** Conceptualization, Methodology, Writing – review & editing, Funding acquisition, Supervision.

Declaration of competing interest

The authors declare that they have no known competing financial interests or personal relationships that could have appeared to influence the work reported in this paper.

Data availability

Data will be made available on request.

Acknowledgments

This work was supported by the National Key Research and Development Program of China (grant number 2019YFD0901401); National Natural Science Foundation of China (grant numbers 11671260; 12071293; 41506194); Natural Sciences and Engineering Research Council of Canada (grant numbers RGPIN-2020-03911, RGPAS-2020-00090).

Appendix A. Supplementary data

Supplementary material related to this article can be found online at https://doi.org/10.1016/j.jtbi.2024.111739.

References

Adhurya, S., Das, S., Ray, S., Fath, B.D., 2021. Simulating the effects of aquatic avifauna on the Phosphorus dynamics of aquatic systems. Ecol. Model. 445, 109495. http://dx.doi.org/10.1016/j.ecolmodel.2021.109495.

Anderson, D., 1997. Turning back the harmful red tide. Nature 388 (6642), 513–514. http://dx.doi.org/10.1038/41415.

Anderson, D.M., Cembella, A.D., Hallegraeff, G.M., 2012. Progress in understanding harmful algal blooms: paradigm shifts and new technologies for research, monitoring, and management. Annu. Rev. Mar. Sci. 4, 143–176. http://dx.doi.org/10.1146/annurev-marine-120308-081121.

Bonachela, J.A., Raghib, M., Levin, S.A., 2011. Dynamic model of flexible phytoplankton nutrient uptake. Proc. Natl. Acad. Sci. 108 (51), 20633–20638. http://dx.doi.org/10.1073/pnas.1118012108.

Bortz, D.M., Nelson, P.W., 2004. Sensitivity analysis of a nonlinear lumped parameter model of HIV infection dynamics. Bull. Math. Biol. 66 (5), 1009–1026. http://dx.doi.org/10.1016/j.bulm.2003.10.011.

Caperon, J., 1969. Time lag in population growth response of Isochrysis galbana to a variable nitrate environment. Ecology 50 (2), 188–192. http://dx.doi.org/10.2307/1934845.

Cunningham, A., Maas, P., 1978. Time lag and nutrient storage effects in the transient growth response of *Chlamydomonas reinhardii* in nitrogen-limited batch and continuous culture. Microbiology 104 (2), 227–231. http://dx.doi.org/10.1099/00221287-104-2-227.

Davies, C.M., Wang, H., 2021. Contrasting stoichiometric dynamics in terrestrial and aquatic grazer–producer systems. J. Biol. Dyn. 15 (sup1), S3–S34. http://dx.doi.org/10.1080/17513758.2020.1771442.

Droop, M., 1973. Some thoughts on nutrient limitation in algae. J. Phycol. 9 (3), 264–272. http://dx.doi.org/10.1111/j.1529-8817.1973.tb04092.x.

Droop, M., 1983. 25 Years of algal growth kinetics a personal view. Bot. Mar. 26 (3), 99–112. http://dx.doi.org/10.1515/botm.1983.26.3.99.

Duan, Z.P., Tan, X., Shi, L., Zeng, Q.F., Ali, I., Zhu, R., Chen, H.M., Parajuli, K., 2023. Phosphorus accumulation in extracellular polymeric substances (EPS) of colony-forming cyanobacteria challenges imbalanced nutrient reduction strategies in Eutrophic Lakes. Environ. Sci. Technol. http://dx.doi.org/10.1021/acs.est.2c04398.

Esmaeili, S., Hastings, A., Abbott, K., Machta, J., Nareddy, V., 2022. Noise-induced versus intrinsic oscillation in ecological systems. Ecol. Lett. 25 (4), 814–827. http://dx.doi.org/10.1111/ele.13956.

Flynn, K.J., Fasham, M.J., Hipkin, C.R., 1997. Modelling the interactions between ammonium and nitrate uptake in marine phytoplankton. Phil. Trans. R. Soc. B 352 (1361), 1625–1645. http://dx.doi.org/10.1098/rstb.1997.0145.

Fu, F.X., Zhang, Y.H., Feng, Y.Y., Hutchins, D.A., 2006. Phosphate and ATP uptake and growth kinetics in axenic cultures of the cyanobacterium *Synechococcus* CCMP 1334. Eur. J. Phycol. 41 (1), 15–28. http://dx.doi.org/10.1080/09670260500505037.

Fu, F.X., Zhang, Y.H., Leblanc, K., Sañudo-Wilhelmy, S.A., Hutchins, D.A., 2005. The biological and biogeochemical consequences of phosphate scavenging onto phytoplankton cell surfaces. Limnol. Oceanogr. 50 (5), 1459–1472. http://dx.doi.org/10.4319/lo.2005.50.5.1459.

Gao, S.F., Shen, A.L., Jiang, J., Wang, H., Yuan, S.L., 2022. Kinetics of phosphate uptake in the dinoflagellate *Karenia mikimotoi* in response to phosphate stress and temperature. Ecol. Model. 468, 109909. http://dx.doi.org/10.1016/j.ecolmodel.2022.109909.

Gómez, F., Zhang, H., Rosellt, L., Lin, S.J., 2021. Detection of *Prorocentrum shikokuense* in the Mediterranean Sea and evidence that *P. dentatum*, *P. obtusidens* and *P. shikokuense* are three different species (Prorocentrales, Dinophyceae). Acta Protozool. 60, 47–59. http://dx.doi.org/10.4467/16890027AP.21.006.15380.

Guillard, R.R.L., 1975. Culture of phytoplankton for feeding marine invertebrates. In: Culture of Marine Invertebrate Animals. Springer, pp. 29–60. http://dx.doi.org/10.1007/978-1-4615-8714-9_3.

Hallegraeff, G.M., 1993. A review of harmful algal blooms and their apparent global increase. Phycologia 32 (2), 79–99. http://dx.doi.org/10.2216/i0031-8884-32-2-79.1.

Huisman, J., Thi, N., Karl, D.M., Sommeijer, B., 2006. Reduced mixing generates oscillations and chaos in the oceanic deep chlorophyll maximum. Nature 439 (7074), 322–325. http://dx.doi.org/10.1038/NATURE04245.

Jiang, J., Shen, A.L., Wang, H., Yuan, S.L., 2019. Regulation of phosphate uptake kinetics in the bloom-forming dinoflagellates *Prorocentrum donghaiense* with emphasis on two-stage dynamic process. J. Theoret. Biol. 463, 12–21. http://dx.doi.org/10.1016/j.jtbi.2018.12.011.

Jin, J., Liu, S.M., Ren, J.L., 2021. Phosphorus utilization by phytoplankton in the Yellow Sea during spring bloom: Cell surface adsorption and intracellular accumulation. Mar. Chem. 231, 103935. http://dx.doi.org/10.1016/j.marchem.2021.103935.

John, E.H., Flynn, K.J., 2000. Modelling phosphate transport and assimilation in microalgae; how much complexity is warranted? Ecol. Model. 125 (2–3), 145–157. http://dx.doi.org/10.1016/S0304-3800(99)00178-7.

Kamennaya, N.A., Geraki, K., Scanlan, D.J., Zubkov, M.V., 2020. Accumulation of ambient phosphate into the periplasm of marine bacteria is proton motive force dependent. Nature Commun. 11 (1), 2642. http://dx.doi.org/10.1038/s41467-020-16428-w.

Kilham, P., Hecky, R.E., 1988. Comparative ecology of marine and freshwater phytoplankton. Limnol. Oceanogr. 33 (4part2), 776–795. http://dx.doi.org/10.4319/lo.1988.33.4part2.0776.

Lin, S.J., Litaker, R.W., Sunda, W.G., 2016. Phosphorus physiological ecology and molecular mechanisms in marine phytoplankton. J. Phycol. 52 (1), 10–36. http://dx.doi.org/10.1111/jpy.12365.

Lin, J.N., Song, J.J., Yan, T., Zhang, Q.C., Zhou, M.J., 2015. Large-scale dinoflagellate bloom species *Prorocentrum donghaiense* and *Karenia mikimotoi* reduce the survival and reproduction of copepod *Calanus sinicus*. J. Mar. Biol. Assoc. UK 95 (6), 1071–1079. http://dx.doi.org/10.1017/S0025315415000533.

Lin, J.N., Yan, T., Zhang, Q., Wang, Y.F., Liu, Q., Zhou, M.J., 2014. In *situ* detrimental impacts of *Prorocentrum donghaiense* blooms on zooplankton in the East China Sea. Mar. Pollut. Bull. 88 (1–2), 302–310. http://dx.doi.org/10.1016/j.marpolbul.2014.08.026.

Lu, D.D., Goebel, J., 2001. Five red tide species in genus Prorocentrum including the description of *Prorocentrum donghaiense* Lu SP. nov. from the East China Sea. Chin. J. Oceanol. Limn. 19 (4), 337–344 (in Chinese with English abstract). http://dx.doi.org/10.1007/BF02850738.

Lu, S.H., Li, Y., 2006. Nutritional storage ability of four harmful algae from the East China Sea. Chin. J. Process Eng. 6 (3), 439 (in Chinese with English abstract).

Lu, S.H., Ou, L.J., Dai, X.F., Cui, L., Dong, Y.L., Wang, P.B., Li, D.M., Lu, D.D., 2022. An overview of *Prorocentrum donghaiense* blooms in China: Species identification, occurrences, ecological consequences, and factors regulating prevalence. Harmful Algae 114, 102207. http://dx.doi.org/10.1016/j.hal.2022.102207.

Marois, D.E., Mitsch, W.J., 2016. Modeling phosphorus retention at low concentrations in florida everglades mesocosms. Ecol. Model. 319, 42–62. http://dx.doi.org/10.1016/j.ecolmodel.2015.09.024.

Mary, I., Tarran, G.A., Warwick, P.E., Terry, M.J., Scanlan, D.J., Burkill, P.H., Zubkov, M.V., 2008. Light enhanced amino acid uptake by dominant bacterioplankton groups in surface waters of the Atlantic Ocean. FEMS Microbiol. Ecol. 63 (1), 36–45. http://dx.doi.org/10.1111/j.1574-6941.2007.00414.x.

Muhammadu, B., Ranganathan, P., Brennan, F., 2017. Dynamic modelling of microalgae cultivation process in high rate algal wastewater pond. Algal Res. 24, 457–466. http://dx.doi.org/10.1016/j.algal.2016.10.016.

Ou, L.J., Wang, D., Huang, B.Q., Hong, H.S., Qi, Y.Z., Lu, S.H., 2008. Comparative study of phosphorus strategies of three typical harmful algae in Chinese coastal waters. J. Plankton Res. 30 (9), 1007–1017. http://dx.doi.org/10.1093/plankt/fbn058.

Qu, Y., Jin, J., Xu, W., Liu, S., 2020. Phosphorus assimilation process by dominant algae species in Chinese coastal sea. China Environ. Sci. 40 (3), 1257–1265 (in Chinese with English abstract).

Sañudo-Wilhelmy, S.A., Tovar-Sanchez, A., Fu, F.X., Capone, D.G., Carpenter, E.J., Hutchins, D.A., 2004. The impact of surface-adsorbed phosphorus on phytoplankton redfield stoichiometry. Nature 432 (7019), 897–901. http://dx.doi.org/10.1038/nature03125.

Saxton, M.A., Arnold, R.J., Bourbonniere, R.A., Mckay, R.M., Wilhelm, S.W., 2012. Plasticity of total and intracellular phosphorus quotas in *Microcystis aeruginosa* cultures and lake erie algal assemblages. Front. Microbiol. 3, 3. http://dx.doi.org/10.3389/fmicb.2012.00003.

Schindler, D.W., Hecky, R.E., Findlay, D.L., Stainton, M.P., Parker, B.R., Paterson, M.J., Beaty, K.G., Lyng, M., Kasian, S.E.M., 2008. Eutrophication of lakes cannot be controlled by reducing nitrogen input: results of a 37-year whole-ecosystem experiment. Proc. Natl. Acad. Sci. 105 (32), 11254–11258. http://dx.doi.org/10.1073/pnas.0805108105.

Shen, A.L., Chen, W.W., Xu, Y.J., Ho, K.C., 2022. Zooplankton population and community structure changes in response to a harmful algal bloom caused by *Prorocentrum donghaiense* in the East China Sea. J. Mar. Sci. Eng. 10 (2), 291. http://dx.doi.org/10.3390/jmse10020291.

Shen, A.L., Gao, S.F., Heggerud, C.M., Wang, H., Ma, Z.L., Yuan, S.L., 2023. Fluctuation of growth and photosynthetic characteristics in *Prorocentrum shikokuense* under phosphorus limitation: Evidence from field and laboratory. Ecol. Model. 479, 110310. http://dx.doi.org/10.1016/j.ecolmodel.2023.110310.

Shen, A.L., Ishizaka, J.J., Yang, M.M., Ouyang, L.L., Yin, Y., Ma, Z.L., 2019. Changes in community structure and photosynthetic activities of total phytoplankton species during the growth, maintenance, and dissipation phases of a *Prorocentrum donghaiense* bloom. Harmful Algae 82, 35–43. http://dx.doi.org/10.1016/j.hal.2018.12.007.

Shen, A.L., Ma, Z.L., Jiang, K.J., Li, D.J., 2016. Effects of temperature on growth, photophysiology, Rubisco gene expression in *Prorocentrum donghaiense* and *Karenia mikimotoi*. Ocean Sci. J. 51 (4), 581–589. http://dx.doi.org/10.1007/s12601-016-0056-2.

Shi, P.L., Shen, H., Wang, W.J., Chen, W.J., Xie, P., 2015. The relationship between light intensity and nutrient uptake kinetics in six freshwater diatoms. J. Environ. Sci. 34, 28–36. http://dx.doi.org/10.1016/j.jes.2015.03.003.

Solovchenko, A.E., Ismagulova, T.T., Lukyanov, A.A., Vasilieva, S.G., Gorelova, O.A., 2019. Luxury phosphorus uptake in microalgae. J. Appl. Phycol. 31 (5), http://dx.doi.org/10.1007/s10811-019-01831-8.

Song, D., Fan, M., Chen, M., Wang, H., 2019. Dynamics of a periodic stoichiometric model with application in predicting and controlling algal bloom in Bohai Sea off China. Math. Biosci. Eng. 16 (1), 119–138. http://dx.doi.org/10.3934/mbe.2019006.

Tester, P.A., Steidinger, K.A., 1997. *Gymnodinium breve* red tide blooms: initiation, transport, and consequences of surface circulation. Limnol. Oceanogr. 42 (5part2), 1039–1051. http://dx.doi.org/10.4319/lo.1997.42.5_part_2.1039.

Tiwari, P.K., Misra, A.K., Venturino, E., 2017. The role of algae in agriculture: a mathematical study. J. Biol. Phys. 43 (2), 297–314. http://dx.doi.org/10.1007/s10867-017-9453-8.

Uye, S., Iwamoto, N., Ueda, T., Tamaki, H., Nakahira, K., 1999. Geographical variations in the trophic structure of the plankton community along a eutrophic–mesotrophic–oligotrophic transect. Fish. Oceanogr. 8 (3), 227–237. http://dx.doi.org/10.1046/j.1365-2419.1999.00110.x.

Wang, H., Garcia, P.V., Ahmed, S., Heggerud, C.M., 2022. Mathematical comparison and empirical review of the monod and droop forms for resource-based population dynamics. Ecol. Model. 466, 109887. http://dx.doi.org/10.1016/j.ecolmodel.2022.109887.

Wang, H., Kuang, Y., Loladze, I., 2008. Dynamics of a mechanistically derived stoichiometric producer-grazer model. J. Biol. Dyn. 2 (3), 286–296. http://dx.doi.org/10.1080/17513750701769881.

Wang, H., Smith, H.L., Kuang, Y., Elser, J.J., 2007. Dynamics of stoichiometric bacteria-algae interactions in the epilimnion. SIAM J. Appl. Math. 68 (2), 503–522. http://dx.doi.org/10.1137/060665919.

Xiao, X., Agusti, S., Pan, Y.R., Yan, Y., Li, K., Wu, J.P., Duarte, C.M., 2019. Warming amplifies the frequency of harmful algal blooms with eutrophication in Chinese Coastal Waters. Environ. Sci. Technol. 2019 (53), 13031–13041. http://dx.doi.org/10.1021/acs.est.9b03726.

Xing, Y.F., Guo, L., Wang, Y., Zhao, Y.G., Jin, C.J., Gao, M.C., Ji, J.Y., She, Z.L., 2021. An insight into the phosphorus distribution in extracellular and intracellular cell of *Chlorella vulgaris* under mixotrophic cultivation. Algal Res. 60, 102482. http://dx.doi.org/10.1016/j.algal.2021.102482.

Xu, W.Q., Liu, S.M., 2016. Phytoplankton responses to phosphorus in Sanggou Bay in spring and autumn. Adv. Mar. Sci. 3 (2), 26–37. http://dx.doi.org/10.12677/ams.2016.32005.

Xu, C.Q., Yuan, S.L., Zhang, T.H., 2021. Competitive exclusion in a general multi-species chemostat model with stochastic perturbations. Bull. Math. Biol. 83 (1), 1–17. http://dx.doi.org/10.1007/s11538-020-00843-7.

Yan, Y.W., Zhang, J.M., Wang, H., 2022. Dynamics of stoichiometric autotroph–mixotroph–bacteria interactions in the epilimnion. Bull. Math. Biol. 84, 1–30. http://dx.doi.org/10.1007/s11538-021-00962-9.

Yang, J.G., Yuan, S.L., 2021. Dynamics of a toxic producing phytoplankton-zooplankton model with three-dimensional patch. Appl. Math. Lett. 118 (3), http://dx.doi.org/10.1016/j.aml.2021.107146.

Yao, B., Xi, B.D., Hu, C.M., Huo, S.L., Shu, J., Liu, H.L., 2011. A model and experimental study of phosphate uptake kinetics in algae: considering surface adsorption and P-stress. J. Environ. Sci. 23 (2), 189–198. http://dx.doi.org/10.1016/S1001-0742(10)60392-0.

Yu, R.C., Zhang, Q.C., Kong, F.Z., Zhou, Z.X., Chen, Z.F., Zhao, Y., Geng, H.X., Dai, L., Yan, T., Zhou, M.J., 2017. Status, impacts and long-term changes of harmful algal blooms in the sea area adjacent to the Changjiang River estuary. Oceanol. Limnol. Sin. 48, 1178–1186 (in Chinese with English abstract).

Yuan, S.L., Wu, D.M., Lan, G.J., Wang, H., 2020. Noise-induced transitions in a nonsmooth Producer–Grazer model with stoichiometric constraints. Bull. Math. Biol. 82 (5), 1–22. http://dx.doi.org/10.1007/s11538-020-00733-y.

Zhang, H.L., Fang, W., Wang, Y.P., Sheng, G.P., Zeng, R.J., Li, W.W., Yu, H.Q., 2013. Phosphorus removal in an enhanced biological phosphorus removal process: roles of extracellular polymeric substances. Environ. Sci. Technol. 47 (20), 11482–11489. http://dx.doi.org/10.1021/es403227p.

Zhao, S.N., Yuan, S.L., Wang, H., 2020. Threshold behavior in a stochastic algal growth model with stoichiometric constraints and seasonal variation. J. Differential Equations 268 (9), 5113–5139. http://dx.doi.org/10.1016/j.jde.2019.11.004.

Zhou, Y., Nguyen, B.T., Zhou, C., Straka, L., Lai, Y.J.S., Xia, S.Q., Rittmann, B.E., 2017a. The distribution of phosphorus and its transformations during batch growth of *Synechocystis*. Water Res. 122, 355–362. http://dx.doi.org/10.1016/j.watres.2017.06.017.

Zhou, Z.X., Yu, R.C., Zhou, M.J., 2017b. Resolving the complex relationship between harmful algal blooms and environmental factors in the coastal waters adjacent to the Changjiang River estuary. Harmful Algae 62, 60–72. http://dx.doi.org/10.1016/j.hal.2016.12.006.

Zubkov, M.V., 2014. Faster growth of the major prokaryotic versus eukaryotic CO2 fixers in the oligotrophic ocean. Nature. Commun. 5 (1), 3776. http://dx.doi.org/10.1038/ncomms4776.

Zubkov, M.V., Martin, A.P., Hartmann, M., Grob, C., Scanlan, D.J., 2015. Dominant oceanic bacteria secure phosphate using a large extracellular buffer. Nature. Commun. 6 (1), 7878. http://dx.doi.org/10.1038/ncomms8878.